Cellular/Molecular

The Arp2/3 Complex Is Essential for Distinct Stages of Spine Synapse Maturation, Including Synapse Unsilencing

Erin F. Spence,[1]* Daniel J. Kanak,[1]* Benjamin R. Carlson,[1] and Scott H. Soderling[1,2]
Departments of [1]Cell Biology and [2]Neurobiology, Duke University Medical School, Durham, North Carolina 27710

Dendritic filopodia are actin-rich structures that are thought to contribute to early spine synapse formation; however, the actin regulatory proteins important for early synaptogenesis are poorly defined. Using organotypic hippocampal slice cultures and primary neuron hippocampal cultures from *Arp2/3* conditional knock-out mice, we analyze the roles of the Arp2/3 complex, an actin regulator that creates branched actin networks, and demonstrate it is essential for distinct stages of both structural and functional maturation of excitatory spine synapses. Our data show that initially the Arp2/3 complex inhibits the formation of dendritic filopodia but that later during development, the Arp2/3 complex drives the morphological maturation from filopodia to typical spine morphology. Furthermore, we demonstrate that although the Arp2/3 complex is not required for key spine maturation steps, such as presynaptic contact and recruitment of MAGUK (membrane-associated guanylate kinase) scaffolding proteins or NMDA receptors, it is necessary for the recruitment of AMPA receptors. This latter process, also known as synapse unsilencing, is a final and essential step in the neurodevelopment of excitatory postsynaptic synaptogenesis, setting the stage for neuronal interconnectivity. These findings provide the first evidence that the Arp2/3 complex is directly involved in functional maturation of dendritic spines during the developmental period of spinogenesis.

Key words: actin; AMPA receptors; Arp2/3; dendritic spine; spinogenesis; synapse unsilencing

Significance Statement

Excitatory spine synapse formation (spinogenesis) is a poorly understood yet pivotal period of neurodevelopment that occurs within 2–3 weeks after birth. Neurodevelopmental disorders such as intellectual disability and autism are characterized by abnormal spine structure, which may arise from abnormal excitatory synaptogenesis. The initial stage of spinogenesis is thought to begin with the emergence of actin-rich dendritic filopodia that initiate contact with presynaptic axonal boutons. However, it remains enigmatic how actin cytoskeletal regulation directs dendritic filopodial emergence or their subsequent maturation into dendritic spines during development and on into adulthood. In this study, we provide the first evidence that the Arp2/3 complex, a key actin nucleator, is involved in distinct stages of spine formation and is required for synapse unsilencing.

Introduction

During the early postnatal period, neurons undergo a rapid and dramatic developmental program of excitatory synapse formation. At the postsynaptic side, this process is thought to begin with the exuberant formation of thin filopodial protrusions from the dendritic shaft that initiate and select for appropriate axonal presynaptic contacts (Ziv and Smith, 1996; Lohmann and Bonhoeffer, 2008). After the stabilization of these contacts, filopodia recruit signaling molecules, membrane-associated guanylate kinase (MAGUK) family scaffolding proteins, and NMDA-type glutamate receptors and expand structurally at their tips into mature dendritic spine heads connected to the dendrite by a thin (~200 nm) neck (Hlushchenko et al., 2016). The "mushroom" morphology of the dendritic spine serves as a biochemical and electrical filter that imparts computational properties of synaptic inputs onto dendrites (Yuste, 2013). In the final stages of spine maturation, the recruitment of AMPA-type glutamate receptors transitions glutamatergic transmission from a "silent" (as a result of the voltage-dependent blockage of NMDA-type receptors) to an "unsilenced" synapse (Isaac et al., 1995; Liao et al., 1995). Misregulation of spinogenesis may underlie several neurodevelopmental disorders such as autism and intellectual disability; however, it is a poorly understood process. Much like dendritic spines, dendritic filopodia are also highly actin rich (Korobova

Received March 16, 2016; revised July 8, 2016; accepted Aug. 2, 2016.

Author contributions: E.F.S., D.J.K., B.R.C., and S.H.S. designed research; E.F.S., D.J.K., and B.R.C. performed research; E.F.S., D.J.K., B.R.C., and S.H.S. analyzed data; E.F.S., D.J.K., and S.H.S. wrote the paper.

This work was supported by National Institutes of Health Grants MH103374 (S.H.S.), NS059957 (S.H.S.), and F31NS092402 (E.F.S.). We thank Il Hwan Kim and Akiyoshi Uezu for technical support and advice and Dr. Cord Brakebusch for providing *Rac1*$^{fl/fl}$ mice.

*E.F.S. and D.J.K. contributed equally to this work.

The authors declare no competing financial interests.

Correspondence should be addressed to Scott H. Soderling at the above address. E-mail: scott.soderling@dm.duke.edu.

DOI:10.1523/JNEUROSCI.0876-16.2016

 0270-6474/16/369696-14$15.00/0

and Svitkina, 2010), and yet the actin-dependent mechanisms regulating the emergence of filopodia and their transition to functional spines during synaptogenesis are poorly defined.

Actin-rich filopodia are common in many cell types and serve as transient sensors of the extracellular environment, including those found at the tips of growth cones of extending axons during embryonic neural development (Gallo and Letourneau, 2004). One striking difference between filopodia of dendrites versus filopodia from other cells types or even neuronal growth cones is the apparent underlying structure of the actin filaments that supports them. In all other known examples, the filopodial cytoskeleton is composed of linear bundled filaments of unidirectional actin that are assembled by nucleators of linear actin such as formins downstream of Rho-family GTPases (Peng et al., 2003; Pellegrin and Mellor, 2005; Schirenbeck et al., 2005). In contrast, dendritic filopodia are unique, with an unusual actin organization composed of filaments of mixed polarity that is branched rather than linear (Korobova and Svitkina, 2010). This has led to the suggestion that the cytoskeleton of dendritic filopodia may be constructed by a different actin nucleator, the Arp2/3 complex. The Arp2/3 complex is composed of seven subunits (Arp2, Arp3, ArpC1, ArpC2, ArpC3, ArpC4, and ArpC5) whose confirmation is switched to an activated state by binding to proteins such as WAVE family proteins downstream of active Rac1 (Soderling and Scott, 2006). Once activated, Arp2/3 initiates the *de novo* actin filament growth off an existing actin filament, leading to the formation of branched actin structures. In mature dendritic spines, the Arp2/3 complex plays a central role in actin remodeling that is essential for spine structural plasticity as well as dendritic spine stability *in vivo* (Kim et al., 2013, 2015). However, the role of the Arp2/3 complex during spinogenesis is less clear, particularly its role in both the structural and functional transition of postsynaptic filopodia formation to spine synapses.

In this study, we show that the Arp2/3 complex plays unexpected and essential roles in both morphological and functional dendritic spine formation and maturation. Using conditional knock-out (KO) mice for *ArpC3*, a critical subunit of the Arp2/3 complex, we show that loss of Arp2/3 activity before the initiation of spinogenesis leads to greater rather than fewer dendritic filopodia, demonstrating that the formation of filopodia does not require Arp2/3 activity. In contrast, Arp2/3 activity is required for the both the structural transition of filopodia to spines and the recruitment of AMPA-type glutamate receptors that is essential for synapse unsilencing during development. These results reveal new insights into the role of actin remodeling during early stages of excitatory synapse formation and suggest there is a tight interplay between the modulation of Arp2/3 activity and early spine development.

Materials and Methods

Animals. Conditional *ArpC3* knock-out animals ($ArpC3^{f/f}$) and conditional *Rac1* knock-out animals ($Rac1^{f/f}$) have been described previously (Chrostek et al., 2006; Kim et al., 2013). Mice of both sexes were used for all experiments. All mice were housed (three to five mice per cage) in the Duke University's Division of Laboratory Animal Resources facilities. All procedures were conducted with a protocol approved by the Duke University Institutional Animal Care and Use Committee in accordance with National Institutes of Health guidelines.

Slice culture. Slices were created from postnatal day 0 (P0) $ArpC3^{f/f}$ pups as described previously (Soderling et al., 2003; Kim et al., 2013). Briefly, P0 pups were rapidly decapitated, and the hippocampi were rapidly dissected. Hippocampi were then cut into 350 μm slices with a tissue chopper (Ted Pella) and transferred to membrane inserts (Millipore), which were placed on cultured media. Two days after incubation, cultures were transfected biolistically with a gene gun (Bio-Rad). Bullets for biolistics were prepared as described previously (Kim et al., 2013).

Primary neuronal culture. Primary neuronal hippocampal cultures were made from mice as previously described (Carlson et al., 2011). Briefly, P0 pups were rapidly decapitated, and hippocampal neurons were plated onto poly-L-lysine (Sigma)-treated coverslips and cultured in Neurobasal A medium supplemented with 2% (v/v) B-27 supplement and 1% (v/v) GlutaMAX (Invitrogen). Neuronal transfections were performed with Lipofectamine 2000 (Invitrogen) according to the manufacturer's instructions on day 5 *in vitro* (DIV 5) after plating, with the modification that neurons were only incubated with lipofectamine for 30 min.

Analysis of slice dendritic spine morphology. Hippocampal slices were prepared from $ArpC3^{f/f}$ P0 mice and transfected biolistically as described above. Slices were either transfected with pβA-GFP [wild-type (WT)] or pβA-GFP-Cre bullets at DIV 2. Slices were then fixed with 4% PFA/4% sucrose at DIV 5 or DIV 14 in PBS for 20 min at 37°C. Slices were permeabilized overnight at 4°C with 1% Triton X-100 in PBS and then were blocked for 2 h with 0.2% Triton X-100 and 5% normal goat serum in PBS at room temperature. Samples were then incubated with chicken anti-GFP antibody (Abcam) for three nights at 4°C. After washing three times for 1 h each with PBS-T (PBS containing 0.2% Triton X-100), slices were incubated with Alexa Fluor 488 anti-chicken (Life Technologies) for two nights at 4°C. Slices were washed three times as before, mounted onto glass slides using FluorSave (Calbiochem) aqueous mounting medium, and imaged on a Zeiss LSM 710 confocal microscope. All images were acquired by z-series (0.13 μm intervals) using a 63×/1.4 numerical aperture (NA) oil-immersion objective. Images were then analyzed in ImageJ. Dendritic protrusions were defined as previously published (Carlson et al., 2011), with filopodia defined as protrusions where the head/tip was less than twice the width of the spine neck. Protrusions were defined as spines when the head/tip was more than or equal to twice the width of the spine neck.

Analysis of cultured neuron dendritic spine morphology and filopodia dynamics. Cultured neurons were prepared from $ArpC3^{f/f}$ and $Rac^{f/f}$ P0 mice and lipofectamine transfected as described above. Neurons were transfected with soluble mCherry with (KO) or without (WT) GFP-Cre. Neurons were fixed at DIV 9 or DIV 14 in 4% paraformaldehyde/4% sucrose in PBS for 15 min at 37°C. Coverslips were mounted with FluorSave Reagent (Calbiochem). All images were acquired with a 63×/1.4 NA oil-immersion objective.

FLEx rescue strategy. Hippocampal slices were prepared from $ArpC3^{f/f}$ P0 mice and transfected as described above. Slices were either transfected with pβA-tomato fluorescent protein (TmFP; WT) or pβA-TmFP-Cre bullets at DIV 2. Slices were infected with either FLEx-GFP or FLEx-ArpC3 (Kim et al., 2015) at DIV 10. After 1 week of viral expression, slices were fixed, immunostained, and imaged as described above or used for electrophysiological recordings.

Western blotting. Lysates were prepared from mouse whole brain at P0, P5, P7, P14, P21, and P42. Five micrograms of sample in sample buffer were electrophoresed through a 12% SDS-PAGE gel (Bio-Rad) and transferred onto nitrocellulose membrane (Whatman) in a Bio-Rad Mini-PROTEAN 3. For Western blot analysis, membranes were then blocked in blocking buffer for fluorescent Western blotting (Rockland) for 1 h at room temperature. Primary antibodies against mDia2 (ECM Biosciences), WAVE (Westphal et al., 2000), Arp3 (Abcam), and β-actin (Novus Biologicals) were diluted in 5% blocking buffer and incubated with the membrane overnight at 4°C. The membranes were then washed three times in TBST and probed with a secondary antibody (Alexa Fluor 647; Life Technologies) diluted in blocking buffer. Proteins were detected using the Li-Cor Odyssey Infrared Imaging System and quantified in ImageJ.

Coimmunoprecipitation. Lysates were prepared from mouse P7 whole brain. Lysates were precleared by centrifugation, and WAVE antibody VO59 (Westphal et al., 2000) was added to supernatant with protein G agarose beads (Millipore) at 4°C. The lysates and beads were incubated overnight at 4°C. After incubation, beads and associated proteins were washed at 4°C once in lysis buffer, then three times with lysis buffer with 1 M NaCl, and finally one additional wash with lysis buffer. The sample

buffer was added to beads and heated to 95°C, and Western blots were performed as above.

siRNA. Hippocampal slices were prepared from *ArpC3$^{f/f}$* P0 mice and transfected as described above. Slices were either transfected with pβA-GFP (WT) or pβA-GFP-Cre (KO) and either scrambled siRNA or previously published siRNA against mDia2 (Yang et al., 2007). Slices were fixed with PFA DIV 5, immunostained against GFP, and imaged for morphology as described previously.

Immunohistochemistry. For MAGUK and Bassoon imaging, cultured neurons were prepared from *ArpC3$^{f/f}$* mouse hippocampus and lipofectamine transfected at DIV 5 as described previously. Neurons were transfected with PSD-95-monobody (Gross et al., 2013) and either pβA-TmFP (WT) or pβA-TmFP-Cre (KO). Neurons were fixed and immunostained as described previously against red fluorescent protein and Bassoon. Neurons were imaged as described previously on a Zeiss 710 confocal microscope, and images were analyzed in ImageJ for colocalization between Bassoon and PSD-95 staining. Briefly, dendritic protrusions in secondary and tertiary dendrites of cultured neurons were selected at random as regions of interest blind to the genotype. If the dendritic protrusion contained puncta enriched above background (background defined as levels in the dendritic shaft), for either Bassoon or PSD-95, the protrusion was considered positive for the respective synaptic marker. If the dendritic protrusion contained both PSD-95 and Bassoon signal, the region was defined as colocalized.

Superecliptic pHluorin intensity and fluorescence recovery after photobleaching imaging. Hippocampal slices were prepared from *ArpC3$^{f/f}$* P0 mice and transfected as described above. Slices were transfected with superecliptic pHluorin (SEP)-GluA1, SEP-GluA2, and either pβA-TmFP (WT) or pβA-TmFP-Cre (KO). Slices were imaged live on a Leica SP8 upright confocal microscope. Five days after transfection, membrane inserts were transferred to 5 cm Petri dishes and filled with preheated HEPES-buffered aCSF containing (in mM) 130 NaCl, 20 HEPES, 2 $NaHCO_3$, 25 D-glucose, 2.5 KCl, and 1.25 NaH_2PO_4, pH 7.35. For fluorescence recovery after photobleaching (FRAP) experiments, baseline fluorescent intensities of randomly selected spines were measured three times and then bleached with a 488 nm laser at 100% intensity for five iterations, using a 25×/0.95 HCXIRAPO WATER dipping lens. Recovery of the fluorescence signal on individual spines was measured and collected every 120 s. Background fluorescence was subtracted from that of target spines. Collected data (seven time points) were then normalized to the average intensity of the first three baseline trials. Control unbleached adjacent spines were monitored to ensure that bleaching was restricted to the spine under study.

Electrophysiology. Whole-cell somatic currents were recorded with silver–silver/chloride electrodes in 2–4 MΩ borosilicate glass micropipettes filled with an intracellular solution containing the following (in mM): 135 Cs-methansulfonate, 10 HEPES, 10 phosphocreatine, 8 NaCl, 5 TEA-Cl, 5 QX-314, 4 MgATP, 0.3 EGTA, and 0.3 Na2GTP (305–310 mOsm, pH adjusted to 7.3–7.4 with CsOH). AMPA receptor miniature EPSCs (AMPAR-mEPSCs) were recorded in aCSF containing (in mM) 124 NaCl, 26 $NaHCO_3$, 10 dextrose, 4 $CaCl_2$, 3 KCl, 1.3 $MgS0_4$, 1.25 NaH_2PO_4, 0.1 picrotoxin, 0.05 D-APV, 0.01 bicuculline methiodide, and 0.0005 tetrodotoxin (TTX) warmed to 25–27°C and continuously bubbled with 95:5 O_2/CO_2. Slices were age matched for all recordings. NMDA receptor mEPSCs (NMDAR-mEPSCs) were recorded in APV-free aCSF containing reduced magnesium (50 μM), CNQX (20 μM), glycine (50 μM), and strychnine (2 μM). No corrections were made for the 8.5–9.0 mV estimated liquid junction potentials of these solutions. Minimal stimulation experiments (0.2 Hz, 200 μs pulses, 20–250 uA) were performed in the absence of TTX, using a stimulus isolation unit (Bak Electronics) and concentric bipolar stimulating electrode (FHC). Signals were low-pass filtered (3 kHz), amplified (10× gain), and digitized (50 kHz) using a Multiclamp 700B amplifier and Digidata 1550 analog-to-digital converter controlled via Clampex software (Molecular Devices). Recordings commenced 10–15 min after rupturing gigaohm seals (1–10 MΩ). Throughout the experiments, we monitored seal stability from membrane current responses elicited by brief, hyperpolarizing voltage steps and monitored the stability of current amplitude and frequency using an on-line, threshold-based detection algorithm developed in MATLAB (Mathworks). Current detection for analysis was performed manually off-line using MiniAnalysis software (Synaptosoft), with thresholds 2.5 times the root-mean-square noise of event-free data epochs. Custom MATLAB scripts were also used to generate cumulative probability distributions and biexponential fits for estimating NMDA-mEPSC decay constants.

Statistics. Descriptive and inferential statistics were performed in Excel (Microsoft) or SPSS (IBM). Regressions and analysis were performed in Prism (Graphpad). We compared independent sample means using *t* tests, one-way or two-way ANOVAs as appropriate, and dependent sample means using repeated-measures ANOVAs. Statistically significant *F* values detected in the ANOVAs were followed by α-adjusted *post hoc* tests (Tukey's HSD or planned contrasts, as indicated in the text). We confirmed necessary parametric test assumptions using the Shapiro–Wilk test (normality), Levene's test (error variance homogeneity), and Mauchly's test (error–variance sphericity). Violations in test assumption violations were corrected by transformations when possible; otherwise, the equivalent nonparametric tests were applied instead. Type-1 error rates for all tests were set at 0.05.

Results

Loss of the Arp2/3 complex leads to an increased number of persistent dendritic filopodia

Because of previous work demonstrating that dendritic filopodia and nascent precursor buds along the dendritic shaft contain a cytoskeletal network of branched actin (Korobova and Svitkina, 2010), we hypothesized that loss of the nucleator of branched actin, the Arp2/3 complex, would lead to a significant reduction of filopodia during synaptogenesis. To test this hypothesis, organotypic hippocampal cultures were prepared from *ArpC3$^{f/f}$* pups at P0 as we previously published (Kim et al., 2013). We focused our morphological studies of synaptogenesis within this preparation to analyze its stages within the context of the native neuropil environment. At DIV 2, slices were biolistically transfected with either GFP (WT, *ArpC3$^{f/f}$*) or GFP and Cre-recombinase (KO, *ArpC3$^{f/f}$:Cre+*). Biolistic transfection provides sparse GFP labeling of pyramidal neurons within the CA1 hippocampal region that are either WT (*ArpC3$^{f/f}$*) or KO for ArpC3 (*ArpC3$^{f/f}$:Cre+*; Fig. 1*A*). By 72 h after Cre expression (in this case DIV 5), ArpC3 protein and Arp2/3 complex activity is lost (Kim et al., 2013; Zhou et al., 2013). At this time point, filopodia are forming on the dendrites of pyramidal neurons in the hippocampal slice culture system, a process that will continue through the first 2 weeks of postnatal development (Fig. 1*B*). Confocal imaging of GFP-positive WT and KO neurons at this time point allowed for the analysis of filopodial density in both sets of neurons. We found that when Arp2/3 activity is lost in this sparse subset of neurons, there is a twofold increase in the density of dendritic protrusions when compared with control neurons expressing GFP alone (Fig. 1*C–G*).

This finding was surprising given previous ultrastructural imaging of actin within filopodia from *in vitro* cultured hippocampal neurons suggested that Arp2/3 activity may be required for their formation (Korobova and Svitkina, 2010). Thus, we repeated our analysis in *ArpC3$^{f/f}$* cultured neurons, a system that has been extensively used for morphological studies and has a more gradual progression of spinogenesis (Fig. 2*A*), by transfecting with GFP and Cre-recombinase or GFP alone at DIV 5. Image analysis of neurons at DIV 8 confirmed the loss of ArpC3 results in elevated (75% increase) rather than reduced filopodial formation (Fig. 2*C–E*). Moreover, analysis of *Rac1* cKO (a GTPase that promotes Arp2/3 activation; Fig. 2*B*) neurons also demonstrated that its loss leads to a 41% increase, rather than a decrease, in filopodial formation (Fig. 2*F–H*). Together, these data show that loss of Arp2/3 activity increases the density of dendritic filopodia,

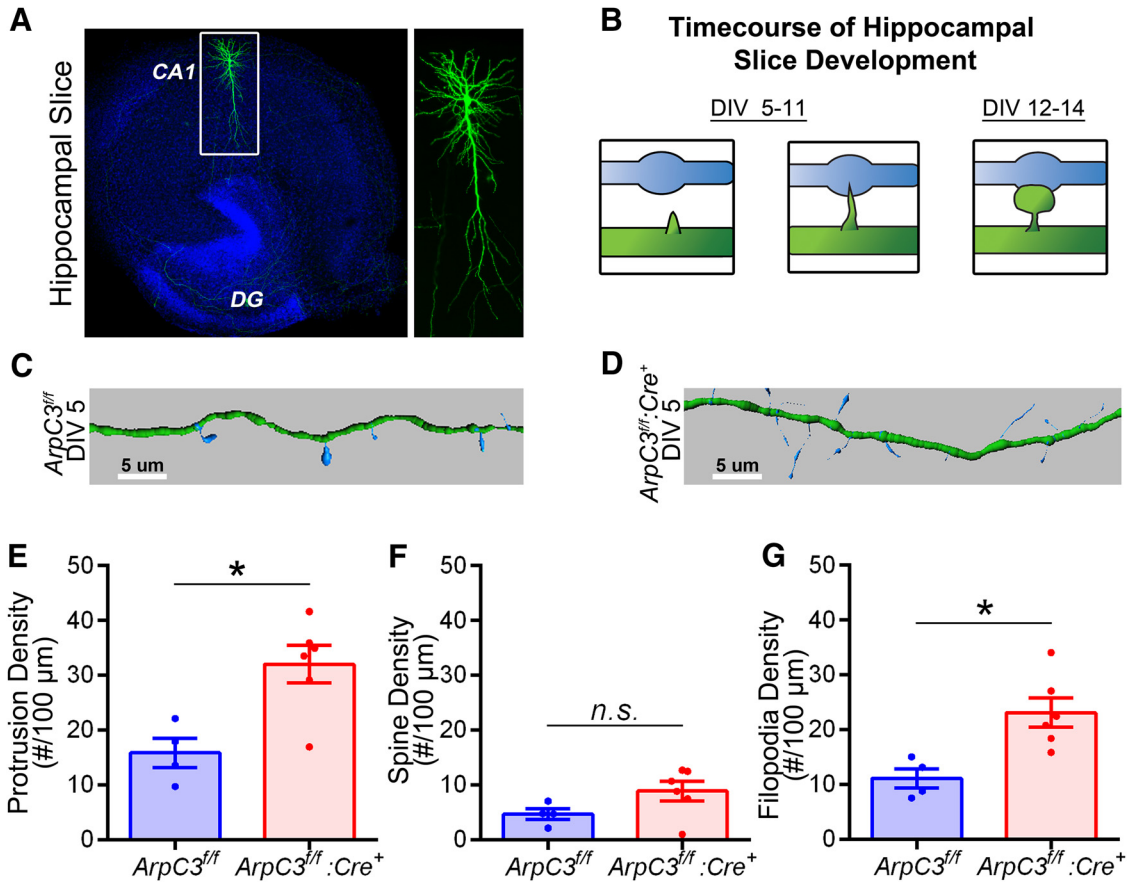

Figure 1. Arp2/3 inhibits initial filopodia formation, yet promotes spine maturation. ***A***, Representative image of a hippocampal slice with sparse biolistic GFP transfection. DG, dentate gyrus. ***B***, Schematic of developmental timeline for morphological maturation of dendritic spines in organotypic hippocampal slice cultures. A dendrite with a developing spine is shown in green, and a presynaptic terminal is shown in blue. ***C***, ***D***, Representative reconstructed confocal images of spine morphology at DIV 5 for *ArpC3$^{f/f}$* (WT; ***C***) and *ArpC3$^{f/f}$:Cre^{+}* (KO; ***D***) neurons. ***E***, Graph depicting protrusion density for WT (16 ± 3 protrusions/100 µm, $n = 4$ slices) versus KO (32 ± 3 protrusions/100 µm, $n = 6$ slices) neurons; $p = 0.010$. ***F***, ***G***, Graphs depicting spine (***F***; WT, 5 ± 1 protrusions/100 µm; KO, 9 ± 2 protrusions/100 µm; $p = 0.113$) and filopodia (***G***; WT, 11 ± 2 protrusions/100 µm; KO, 23 ± 3 protrusions/100 µm; $p = 0.011$) density for WT versus KO neurons. Error bars are SEM. $^{*}p < 0.05$. Scale bars, 5 µm.

demonstrating that Arp2/3 activity is not required for the initial formation of these protrusions.

Loss of the Arp2/3 complex stalls the morphological transition of dendritic filopodia to spines

We next determined whether ArpC3-deficient filopodia could transition into typical morphology of mature dendritic spines characterized by an enlarged spine head, often referred to as mushroom shaped. In cultured neurons, a period of robust morphological change occurs between DIV 12 and DIV 14 (Carlson et al., 2011). To examine the long-term fate of the Arp2/3-deficient dendritic filopodia, we examined the dendritic spine morphology of *ArpC3$^{f/f}$* neurons in hippocampal slices after 2 weeks *in vitro* with and without Cre-recombinase transfection. Because dendritic spines are composed of networks of highly branched actin filaments (Korobova and Svitkina, 2010), we hypothesized that a loss of Arp2/3 would impair the transition between filopodial protrusions to spines with enlarged heads. We imaged WT and KO neurons at DIV 12–14, a time point when dendritic spines are undergoing morphological maturation in hippocampal slices (Figs. 1*B*, 3*A*). Whereas the total number of protrusions between WT and KO neurons did not significantly differ (Fig. 3*C*), there was a significant impairment in the structural maturation of filopodial protrusions into typical spine morphology that was evidenced by a 68% reduction in spine density (Fig. 3*B*,*D*). Specifically, the KO dendrites were decorated with a significantly larger fraction of morphologically immature filopodial-like protrusions (an ~20-fold increase compared with WT; Fig. 3*E*). Together, these data show that although Arp2/3 activity appears to limit filopodial density, it is essential for their subsequent morphological transition into dendritic spines.

To further test the requirement of Arp2/3 activity for the morphological maturation of filopodia into spines, we performed a rescue experiment, reintroducing ArpC3 into Cre-expressing neurons using a FLEx (Schnütgen et al., 2003) adeno-associated viral strategy (Fig. 3*F*), as we previously published (Kim et al., 2015). P0 hippocampal organotypic slice cultures from *ArpC3$^{f/f}$* pups were biolistically transfected with tdTomato or tdTomato-Cre at DIV 2. At DIV 10, during the transition from filopodia to dendritic spines, ArpC3 was virally reintroduced into Cre^{+} neurons. A negative control containing FLEx-GFP without ArpC3 was used to control for effects of viral infection. After 1 week of viral infection, slices were fixed and imaged. WT neurons infected with either FLEx-GFP or FLEx-ArpC3 exhibited a normal density and morphology of dendritic protrusions (Fig. 3*G*,*H*,*K*–*M*). Consistent with previous results, ArpC3 KO neurons infected with FLEx-GFP exhibited a 72% lower density of spines as well as a fourfold increase in morphologically immature filopodial protrusions (Fig. 3*H*,*K*–*M*). ArpC3 KO neurons with ArpC3 re-expression, in contrast, displayed a morphology and

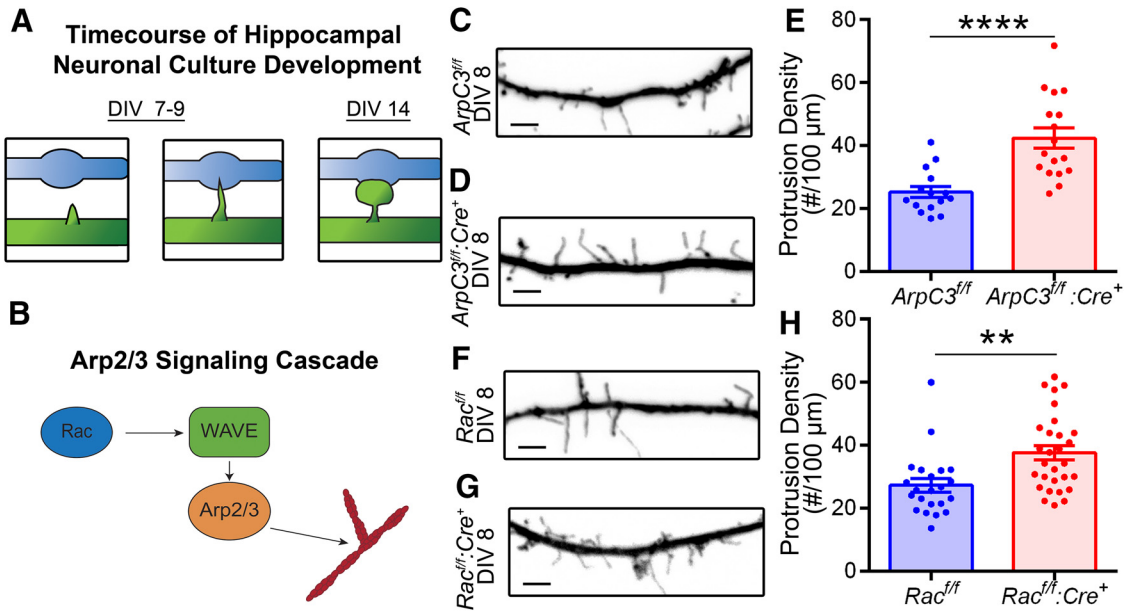

Figure 2. Arp2/3 and Rac inhibit initial filopodia formation in dissociative cultures. ***A***, Schematic of developmental timeline for morphological maturation of dendritic spines in primary hippocampal neuron cultures. A dendrite with a developing spine is shown in green, and a presynaptic terminal is shown in blue. ***B***, Schematic depicting Arp2/3 complex signaling cascade. ***C***, ***D***, Representative confocal images of *ArpC3*$^{f/f}$ (WT) and *ArpC3*$^{f/f}$*:Cre*$^{+}$ (KO) morphology at DIV 8. ***E***, Graph depicting protrusion density for *ArpC3*$^{f/f}$ WT (24 ± 2 protrusions/100 μm, $n = 15$ neurons) versus KO (42 ± 3 protrusions/100 μm, $n = 17$ neurons) neurons; $p < 0.0001$. ***F***, ***G***, Representative confocal images of spine morphology of *Rac*$^{f/f}$ (WT) and *Rac*$^{f/f}$*:Cre*$^{+}$ (KO) morphology at DIV 8. ***H***, Graph depicting protrusion density for *Rac* WT (27 ± 2 protrusions/100 μm, $n = 22$ neurons) versus KO (38 ± 2 protrusions/100 μm; $n = 29$ neurons) neurons; $p = 0.001$. Error bars are SEM. $^{**}p < 0.01$; $^{****}p < 0.0001$. Scale bars, 5 μm.

protrusion density similar to WT neurons (Fig. 3*J–M*). Whereas the rescued neurons were not significantly different from WT neurons, the KO neurons were significantly different from both. Together, these data demonstrate that ArpC3-deficient filopodia are competent to transition into mature dendritic spines but in the absence of Arp2/3 are stalled in a morphologically immature state. Furthermore, the protrusion density data suggest that there is a period in which Arp2/3 supports the transition from morphologically immature to mature spines. If Arp2/3-dependent spine maturation is interrupted, the protrusion density starts to decline (Fig. 3*K*), supporting the notion that morphologically immature spines are less stable (Parnass et al., 2000; Grutzendler et al., 2002; Trachtenberg et al., 2002).

mDia2 drives filopodia formation in the absence of the Arp2/3 complex

Because our data suggest that the Arp2/3 complex functions as a negative regulator of filopodial density during early spinogenesis, we were next interested in determining the positive factor that promotes actin polymerization during the filopodial stage of synaptogenesis in the absence of a functional Arp2/3 complex. Previous work implicated the formin family member mDia2 as an important actin nucleator during dendritic filopodia formation (Hotulainen et al., 2009). Moreover, in non-neuronal cells mDia2 interacts with the Arp2/3 complex via the WAVE family of Arp2/3 activators, and the knockdown of the Arp2/3 complex leads to an expansion of mDia2-mediated filopodia (Beli et al., 2008). As a first step to determine whether a similar functional relationship exists between mDia2 and the Arp2/3 activator WAVE in dendritic filopodia formation, we determined their developmental expression patterns in brain samples. Quantitative Western blot analysis of whole-brain lysates at P0, P5, P7, P14, P21, and P42 showed that WAVE, mDia2, and Arp3 show overlapping but differential patterns of expression during development (Fig. 4*A–D*). mDia2 expression is highest between P0 and P5, when filopodial formation occurs, and starts to decrease around the end of the first postnatal week. In contrast, WAVE expression remains stable during the first postnatal week and increases twofold by P14 during the morphological transition period from filopodia to spines. Furthermore, mDia2 coimmunoprecipitated with WAVE in a pull-down assay from P7 brain lysates (Fig. 4*E*), suggesting that an analogous WAVE–mDia2 interaction occurs. Based on prior work in cultured cells, the differential pattern of expressions, and the presence of the WAVE–mDia2 complex, we hypothesized the loss of Arp2/3 activity might lead to an increased expansion of mDia2-dependent filopodial structures. If correct, the knockdown of mDia2 would normalize the abnormally high density of filopodia observed in the ArpC3 KO neurons. To test this possibility, we first replicated the findings of Hotulainen et al. (2009) in cultured dissociated neurons using siRNA against mDia2 (scrambled siRNA protrusion density: 43 ± 3 protrusion/100 μm, $n = 12$ neurons; mDia2 siRNA protrusion density: 32 ± 2 protrusions/100 μm, $n = 12$ neurons; $p = 0.003$), verifying our siRNA works. Next, hippocampal slice cultures from P0 *ArpC3*$^{f/f}$ pups were biolistically transfected at DIV 2 with either scrambled siRNA or previously published mDia2 siRNA (Yang et al., 2007) along with either GFP-Cre or GFP alone. Slices were fixed and imaged at DIV 5. In the absence of mDia2, there was no difference in filopodia density in WT neurons (contrasting with results from dissociated cultured neurons); however, the increase in the density of filopodia in the ArpC3 KO neurons was abolished (Fig. 4*F–J*). These data demonstrate that in the absence of the Arp2/3 complex from neurons in slice, mDia2 activity mediates the increased density of filopodia, analogous to the expansion of filopodia in non-neuronal cells. However, which proteins are critical for the formation of dendritic filopodia under basal conditions remains unclear.

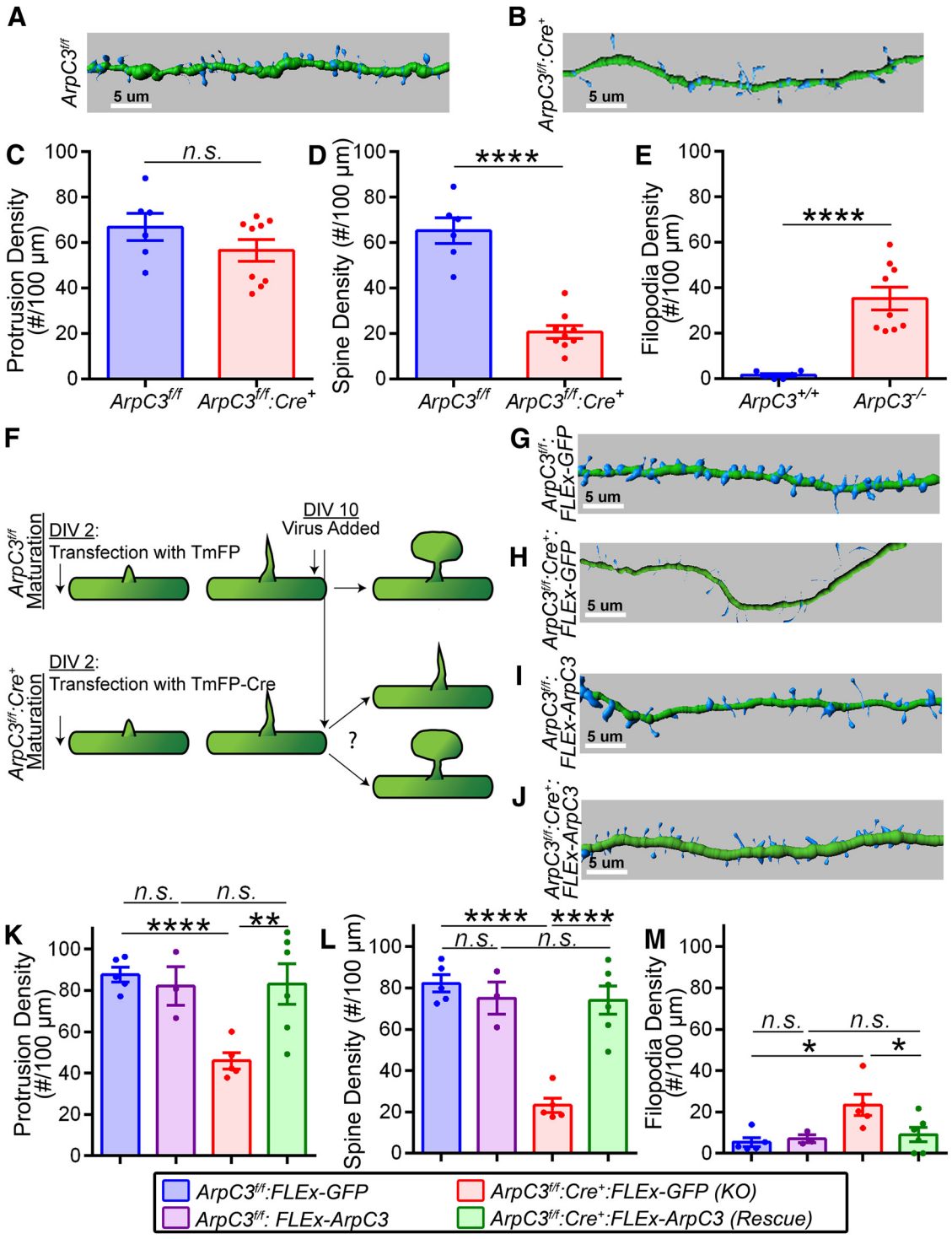

Figure 3. Loss of Arp2/3 activity prevents dendritic spine morphological maturation. ***A***, ***B***, Representative reconstructed confocal images of spine morphology at DIV 12–14 for *ArpC3*$^{f/f}$ (WT; ***A***) and *ArpC3*$^{f/f}$:*Cre*$^{+}$ (KO; ***B***) neurons. ***C***, Graph depicting protrusion density for WT (66 ± 6 protrusions/100 µm, $n = 6$ slices) versus KO (57 ± 5 protrusions/100 µm, $n = 9$ slices) neurons; $p = 0.181$. ***D***, ***E***, Graphs depicting spine (***D***; WT: 65 ± 5 protrusions/100 µm, $n = 6$ slices; KO: 21 ± 3 protrusions/100 µm, $n = 9$ slices; $p < 0.0001$) and filopodia (***E***; WT: 2 ± 1 protrusions/100 µm, $n = 6$ slices; KO: 35 ± 5 protrusions/100 µm, $n = 9$ slices; $p < 0.0001$) density for WT versus KO neurons. ***F***, Experimental timeline for FLEx-ArpC3 morphology rescue experiment. ***G–J***, Representative reconstructed image of GFP-virus control (*ArpC3*$^{f/f}$:*FLEx-GFP*; ***G***), ArpC3-virus control (*ArpC3*$^{f/f}$:*FLEx-ArpC3*; ***H***), ArpC3 KO (*ArpC3*$^{f/f}$:*Cre*$^{+}$:*FLEx-GFP*; ***I***), and ArpC3 Rescue (*ArpC3*$^{f/f}$:*Cre*$^{+}$:*FLEx-ArpC3*; ***J***). ***K***, Graph depicting protrusion density for *ArpC3*$^{f/f}$ versus *ArpC3*$^{f/f}$:*Cre*$^{+}$ neurons with either FLEx-GFP or FLEx-ArpC3. *ArpC3*$^{f/f}$:*FLEx-GFP*: 88 ± 4 protrusions/100 µm, $n = 5$ slices; *ArpC3*$^{f/f}$:*Cre*$^{+}$:*FLEx-GFP*: 82 ± 9 protrusions/100 µm, $n = 3$ slices; *ArpC3*$^{f/f}$:*Cre*$^{+}$:*FLEx-GFP*: 46 ± 4 protrusions/100 µm, $n = 5$ slices; *ArpC3*$^{f/f}$:*Cre*$^{+}$:*FLEx-ArpC3:* 83 ± 10 protrusions/100 µm, $n = 6$ slices. $F_{(3,15)} = 6.965$, $p = 0.008$. ***L***, Graph depicting spine density for *ArpC3*$^{f/f}$ versus *ArpC3*$^{f/f}$:Cre $^{+}$ neurons with either FLEx-GFP or FLEx-ArpC3. *ArpC3*$^{f/f}$:*FLEx-GFP*: 82 ± 4, $n = 5$ slices; *ArpC3*$^{f/f}$:*Cre*$^{+}$:*FLEx-GFP*: 75 ± 8 spines/100 µm, $n = 3$ slices; *ArpC3*$^{f/f}$:*Cre*$^{+}$:*FLEx-GFP*: 23 ± 3 spines/100 µm, $n = 5$ slices; *ArpC3*$^{f/f}$:*Cre*$^{+}$:*FLEx-ArpC3:* 74 ± 7 spines/100 µm, $n = 6$ slices. $F_{(3,15)} = 23.47$, $p < 0.0001$. ***M***, Graph depicting filopodia density for *ArpC3*$^{f/f}$ versus *ArpC3*$^{f/f}$:Cre $^{+}$ neurons with either FLEx-GFP or FLEx-ArpC3. *ArpC3*$^{f/f}$:*FLEx-GFP*: 5 ± 2 filopodia/100 µm, $n = 5$ slices; *ArpC3*$^{f/f}$:*Cre*$^{+}$:*FLEx-GFP*: 7 ± 2 filopodia/100 µm, $n = 3$ slices; *ArpC3*$^{f/f}$:*Cre*$^{+}$:*FLEx-GFP*: 23 ± 5 filopodia/100 µm, $n = 5$ slices; *ArpC3*$^{f/f}$:*Cre*$^{+}$:*FLEx-ArpC3:* 9 ± 4 filopodia/100 µm, $n = 6$ slices. $F_{(3,15)} = 4.868$, $p = 0.054$. Error bars are SEM. *$p < 0.05$; **$p < 0.01$; ****$p < 0.0001$. Scale bars, 5 µm.

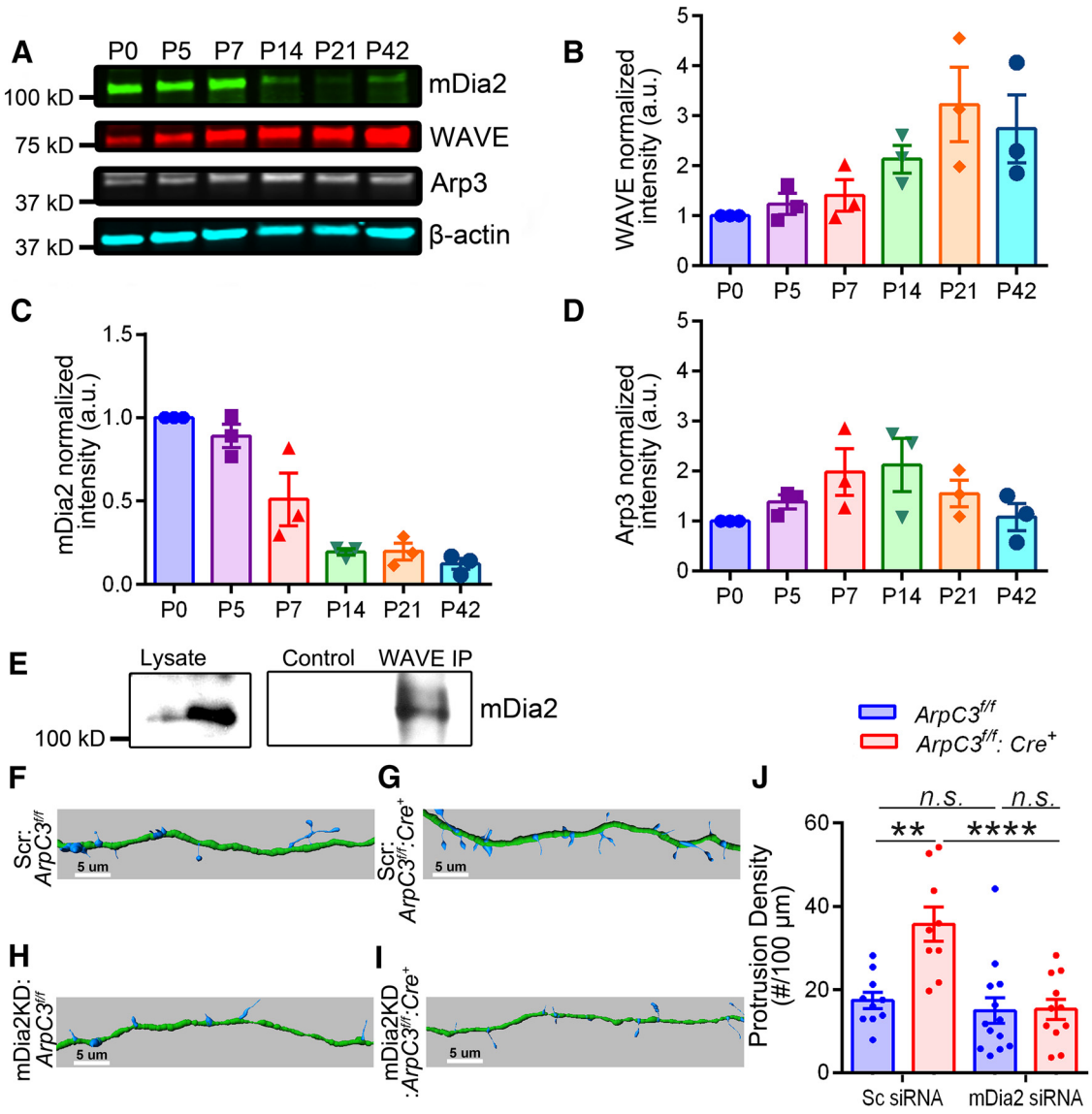

Figure 4. mDia2 interacts with the Arp2/3 activator WAVE and promotes initial dendritic protrusions in the absence of ArpC3. ***A***, Immunoblot analysis of whole-brain lysate for mDia2 expression, WAVE expression, and Arp3 expression at specific developmental time points. Molecular markers of mass are indicated to the left of each immunoblot. β-Actin was used as a loading control. ***B***, Quantification of WAVE relative density adjusted to the β-actin loading control and normalized to P0; $n = 3$ cohorts of mice. P5, 1.28 ± 0.25 a.u.; P7, 1.455 ± 0.36 a.u.; P14, 2.22 ± 0.36 a.u.; P21, 3.35 ± 0.75 a.u.; P42, 2.93 ± 0.86. a.u. ***C***, Quantification of mDia2 relative density adjusted to the β-actin loading control and normalized to P0; $n = 3$ cohorts of mice. P5, 0.93 ± 0.10 a.u.; P7, 0.50 ± 0.15 a.u.; P14, 0.18 ± 0.03 a.u.; P21, 0.21 ± 0.04 a.u.; P42, 0.13 ± 0.04 a.u. ***D***, Quantification of Arp3 relative density adjusted to the β-actin loading control and normalized to P0; $n = 3$ cohorts of mice. P5, 1.87 ± 0.14 a.u.; P7, 1.98 ± 0.47 a.u.; P14, 2.13 ± 0.53 a.u.; P21, 1.56 ± 0.27 a.u.; P42, 1.08 ± 0.27 a.u. ***E***, Left, Immunoblot for mDia2 from whole-brain lysates from P7 mice. Right, Control (IgG alone) and WAVE coimmunoprecipitation (IP) with mDia2. Markers of molecular mass are indicated to the left of each immunoblot. ***F–I***, Representative reconstructed confocal image of WT scrambled RNAi (scRNAi) control (*ArpC3*$^{f/f}$:scRNAi; ***F***), KO scRNAi control (*ArpC3*$^{f/f}$:*Cre*$^{+}$:scRNAi; ***G***), WT mDia2 RNAi knockdown (*ArpC3*$^{f/f}$:mDia2 RNAi; ***H***), and KO mDia2 RNAi knockdown (*ArpC3*$^{f/f}$:*Cre*$^{+}$:mDia2 RNAi; ***I***). ***J***, Graph depicting protrusion density for *ArpC3*$^{f/f}$ versus *ArpC3*$^{f/f}$:*Cre*$^{+}$ neurons with either scRNAi or mDia2 siRNA. *ArpC3*$^{f/f}$:scRNAi: 17 ± 2 protrusions/100 μm, $n = 10$ slices; *ArpC3*$^{f/f}$:*Cre*$^{+}$:scRNAi: 35 ± 4 protrusions/100 μm, $n = 8$ slices; *ArpC3*$^{f/f}$:mDia2 RNAi: 15 ± 3 protrusions/100 μm, $n = 14$ slices; *ArpC3*$^{f/f}$:*Cre*$^{+}$:mDia2 RNAi: 15 ± 3 protrusions/100 μm, $n = 11$ slices. $F_{(1,39)} = 8.956$, $p = 0.017$. Error bars are SEM. $^{**}p < 0.01$; $^{****}p < 0.0001$. Scale bars, 5 μm.

ArpC3 $^{-/-}$ stalled filopodia establish synaptic contacts and recruit MAGUK proteins but do not recruit surface AMPA receptors

Although the above analysis reveals the stages of spinogenesis Arp2/3 is required for during the structural formation and transition of dendritic filopodia to spines, it was still unclear whether Arp2/3-dependent actin is required for specific aspects of the functional maturation of spines. During synaptogenesis, there are several key developmental steps (including presynaptic contact and the recruitment of scaffolding proteins and glutamate receptor recruitment) that are required for the formation of a functional postsynaptic structure. Because Arp2/3-deficient filopodia are morphologically immature, we were interested in determining whether they were able to transition toward functional synaptic contacts. We first analyzed whether ArpC3 KO protrusions were able to establish contacts with presynaptic structures, a step that requires adhesion across the synaptic cleft. Covisualization of presynaptic terminals with dendritic protrusions of either WT or KO neurons revealed that Arp2/3-deficient protrusions established contacts with presynaptic terminals with the same frequency as WT protrusions (Fig. 5*A–C*). We next analyzed the recruitment of MAGUK scaffolding proteins, using a PSD-95-monobody that detects and labels endogenous protein (Gross et al., 2013). This approach was advantageous as it pre-

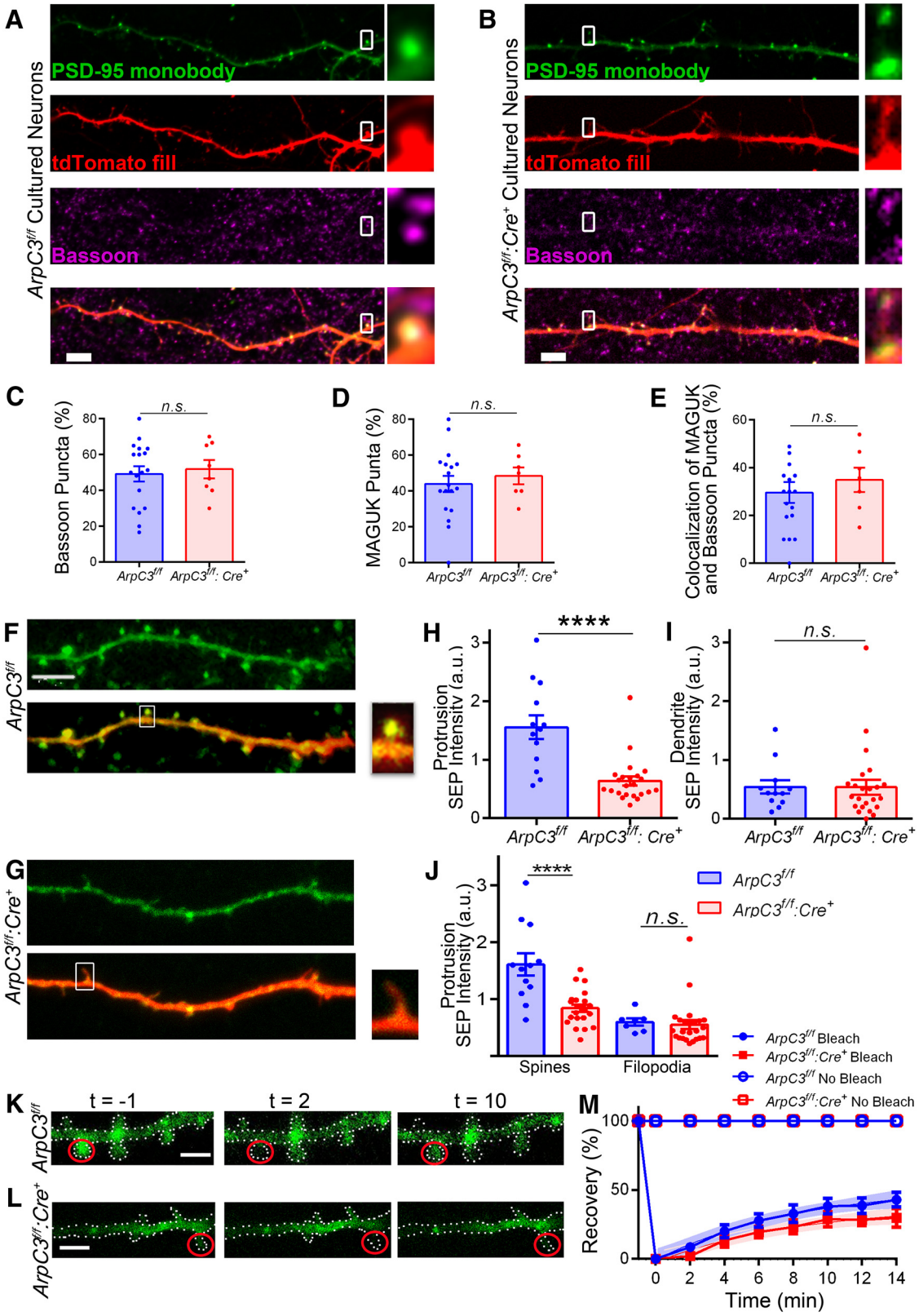

Figure 5. ArpC3-deficient neurons recruit MAGUK proteins and make presynaptic contact but do not enrich synaptic AMPARs. ***A***, ***B***, Representative images of DIV 12 neurons from hippocampal primary cultures. The green signal is PSD-95-monobody-GFP, and the red signal is either tdTomato (WT, *ArpC3*$^{f/f}$; ***A***) or ***x***Cre-2A-tdTomato (KO, *ArpC3*$^{f/f}$:*Cre*$^{+}$; ***B***). The magenta signal is immunofluorescence for the presynaptic marker Bassoon. ***C***, Graph depicting percentage of dendritic protrusions with Bassoon puncta. WT: 49 ± 6 puncta/100 μm, $n = 18$ neurons; KO: 54 ± 10 puncta/100 μm, $n = 8$ neurons; $p = 0.68$. ***D***, Graph depicting percentage of dendritic protrusions with PSD-95-monobody-GFP puncta. WT: 44 ± 5 puncta/100 μm, $n = 18$ neurons; KO: 50 ± 5 puncta/100 μm, $n = 8$ neurons; $p = 0.51$. ***E***, Colocalization of both PSD-95-monobody-GFP and Bassoon puncta. WT: 28 ± 6 puncta/100 μm, $n = 18$; KO: 35 ± 11 puncta/100 μm, $n = 8$; $p = 0.59$. ***F***, ***G***, Representative images of DIV 12–17 slice culture neurons expressing SEP-GluA1 and SEP-GluA2 (1:1 molar ratio) and either tdTomato (*ArpC3*$^{f/f}$; ***F***) or Cre-2A-tdTomato (*ArpC3*$^{f/f}$:*Cre*$^{+}$; ***G***). ***H***, Graph depicting the ratio of protrusion SEP-GluA1/GluA2 intensity to dendrite intensity. WT: 1.52 ± 0.21 a.u., $n = 12$ slices; KO: 0.66 ± 0.08 a.u., $n = 24$ slices, (*Figure legend continues.*)

vents artifact effects of MAGUK overexpression (Nikonenko et al., 2008; Poglia et al., 2011). PSD-95-monobody puncta occurred with the same frequency within dendritic protrusions of WT and KO neurons (Fig. 5*D*) and also colocalized with presynaptic marker Bassoon with the same frequency (Fig. 5*E*). Thus, the loss of Arp2/3 activity does not affect the initial stages of presynaptic contact or MAGUK scaffolding protein recruitment to synaptic structures.

These initial molecular steps of synapse development are thought to precede the final recruitment of AMPA-type glutamate receptors to dendritic spines. This is a critical stage of synapse maturation because the arrival of AMPA receptors marks the transition of spines from functionally silent to functionally active or unsilenced synapses. To determine whether Arp2/3 is required for AMPA receptor recruitment, the surface levels of AMPA receptors at synaptic sites were analyzed at DIV 14 from WT and KO neurons using SEP-tagged GluA1 and GluA2 (Fig. 5*F*, *G*). Quantitative analysis of SEP-GluA1/2 intensity indicated there was a dramatic, 57% decrease in the GluA1/A2 surface enrichment within dendritic protrusions from KO neurons when compared with WT neurons (Fig. 5*H*). This difference is not the result of differences in SEP-GluA1/GluA2 expression because levels of SEP-GluA1/GluA2 in the dendrite remain constant (Fig. 5*I*). Instead, the difference is primarily driven by the intensity difference between WT dendritic spines and the remaining KO dendritic spines (Fig. 5*J*). Filopodia in each group have similarly low levels of GluA1/GluA2 surface enrichment. We next performed FRAP experiments to determine whether Arp2/3 is required for aspects of GluA1/GluA2 turnover at dendritic protrusions (Fig. 5*K–M*). Our results show that the rate of recovery for the first 14 min was similar between WT and KO protrusions (WT: $k = 0.12 \pm 0.1\ \text{min}^{-1}$, $n = 14$ spines; KO: $k = 0.11 \pm 0.1\ \text{min}^{-1}$, $n = 14$ spines; $p = 0.908$; Fig. 5*N*), suggesting that loss of Arp2/3 does not affect initial turnover of AMPA-type glutamate receptors. Together, these data show that Arp2/3 is not required for early maturation steps of functional synapse formation, such as recruiting MAGUKs or establishing presynaptic contacts, but that it is required for the enrichment of surface AMPARs to nascent synapses. To verify the reduced levels of synaptic AMPAR in the ArpC3 null neurons and to establish whether this extended to other ionotropic glutamate receptors, such as NMDARs, we next performed electrophysiological recordings.

ArpC3-deficient protrusions contain NMDARs but do not undergo AMPAR-dependent synapse unsilencing

Later stages of spinogenesis include (1) NMDAR subunit switching from NR2b- to NR2a-containing NMDAR subunits and (2) AMPAR recruitment to the postsynaptic membrane (Monyer et al., 1994; Petralia et al., 2005). These processes result in a developmental switch that effectively transitions a silent synapse, characterized by an increased AMPAR/NMDAR IEI ratio, to an unsilenced synapse that exhibits a decreased AMPAR/NMDAR interevent interval (IEI) ratio (Hanse et al., 2013). Given the lack of AMPAR recruitment evident in our imaging analysis, we sought electrophysiological evidence for a potential role of ArpC3 in synapse unsilencing. To this end, we first assessed IEI ratios of pharmacologically isolated AMPAR- and NMDAR-mEPSCs recorded from WT and ArpC3 KO CA1 pyramidal cells. Performed in biolistically transfected slice cultures prepared from P0 *ArpC3*$^{f/f}$ pups, the results of these experiments predominately reflect the postsynaptic effects of ArpC3 loss within the context of WT Schaffer collateral input (i.e., as a result of the sparse nature of biolistic transfection). The results of our electrophysiology experiments performed between DIV 14 and DIV 21 indicate a significant fivefold increase in the AMPAR/NMDAR-mEPSC IEI ratio in ArpC3 KO versus WT neurons (Fig. 6*A*). Consistent with the SEP-GluA1/2 imaging analysis, the altered IEI ratio in ArpC3 KO neurons exclusively reflects an increase in AMPAR-mEPSC IEI (Fig. 6*B–D*). More specifically, ArpC3 KO neurons exhibited decreased AMPAR-mEPSC frequency, measured as a 392% increase in IEI (Fig. 6*C*), whereas ArpC3 loss had no significant effect on the NMDAR-mEPSC IEIs (Fig. 6*D*). Compared with WT neurons, the median amplitudes of AMPAR-mEPSCs were also reduced by 46% in ArpC3 KO versus WT neurons (Fig. 6*E*), whereas those of NMDAR-mEPSCs were comparable between genotypes (Fig. 6*F*). Comparing NMDAR-mEPSC amplitude-weighted decay constants between WT and ArpC3 KO neurons at DIV 14–21 revealed no significant difference (Fig. 6*G*). As a positive control, we also compared the WT decay kinetics with those of DIV 3–5 WT neurons, a time point during which NMDAR subunits are predominately NR2B containing with faster decay constants. Compared with DIV 14–21 WT neurons, NMDAR-mEPSC decay constants were 69% faster in DIV 3–5 neurons. Therefore, we infer that NR2B to NR2A subunit switching occurs in our preparation and that the process is unaffected by ArpC3 loss. Additional evidence for a "silent synapse" phenotype was obtained by examining the failure rates of evoked AMPAR- and NMDAR-mediated EPSCs during a 0.2 Hz minimal stimulation protocol. The results of these experiments demonstrate an ArpC3-dependent significant threefold increase in AMPAR failure rates unaccompanied by a difference in NMDAR failures (Fig. 6*H*). Together, these data show that Arp2/3 activity exerts a preferential influence on AMPAR recruitment during synapse development.

Previously we had shown that Arp2/3 rescue in KO neurons transitions developmentally "immature" spines into morphologically mature postsynaptic structures. We next asked whether the morphological rescue accompanies a functional rescue of the AMPAR-mEPSC deficit identified in our electrophysiology experiments. To this end, we used the FLEx-ArpC3 viral rescue strategy, allowing 8 d of Cre expression for filopodial formation and presynaptic contact formation to occur in slice culture in the absence of Arp2/3 activity and then allotted an additional 7 d for viral re-expression of ArpC3. This experiment recapitulated the percentage differences in AMPAR-mEPSC amplitudes and IEIs observed in control and KO neurons (amplitude, −40%; IEI, 465%; Fig. 6*I–M*; blue, WT; red, KO). More importantly, when compared with control neurons, viral-mediated re-expression of ArpC3 rescued these deficits (Fig. 6*J–M*; green, rescue). These data suggest that Arp2/3 activity-dependent AMPAR recruitment is more likely involved in later stages of synapse maturation since

←

(*Figure legend continued.*) $p = 0.002$. ***I***, Graph depicting the ratio of SEP intensity to tdTomato intensity in the dendrite. WT: 0.54 ± 0.11 a.u., $n = 12$ slices; KO: 0.54 ± 0.13 a.u., $n = 24$ slices, $p = 0.645$. ***J***, Graph depicting the ratio of spine and filopodia SEP-GluA1/GluA2 intensity to dendrite intensity. WT spines: 1.61 ± 0.20 a.u., $n = 12$ slices; KO spines: 0.84 ± 0.07 a.u., $n = 22$ slices, $p < 0.0001$; WT filopodia: 0.60 ± 0.06 a.u., $n = 7$ slices; KO filopodia: 0.56 ± 0.08 a.u., $n = 24$ slices, $p = 0.35$. ***K***, ***L***, Representative images of DIV 12–17 slice culture neurons expressing SEP-GluA1 and SEP-GluA2 before FRAP ($t = -1$), 2 min after FRAP ($t = 2$), and 10 min after FRAP ($t = 10$). ***M***, Graph depicting percentage recovery of SEP-GluA1/GluA2 fluorescence in photobleached dendritic protrusions after photobleaching over time. $F_{(2,65)} = 0.50$, $p = 0.649$. Shaded regions represent the 95th percentile confidence interval of regression fit. Nonbleached WT and KO protrusion are shown as open circles and squares. Error bars are SEM. $^{**}p < 0.01$; $^{****}p < 0.0001$. Scale bars, 5 μm.

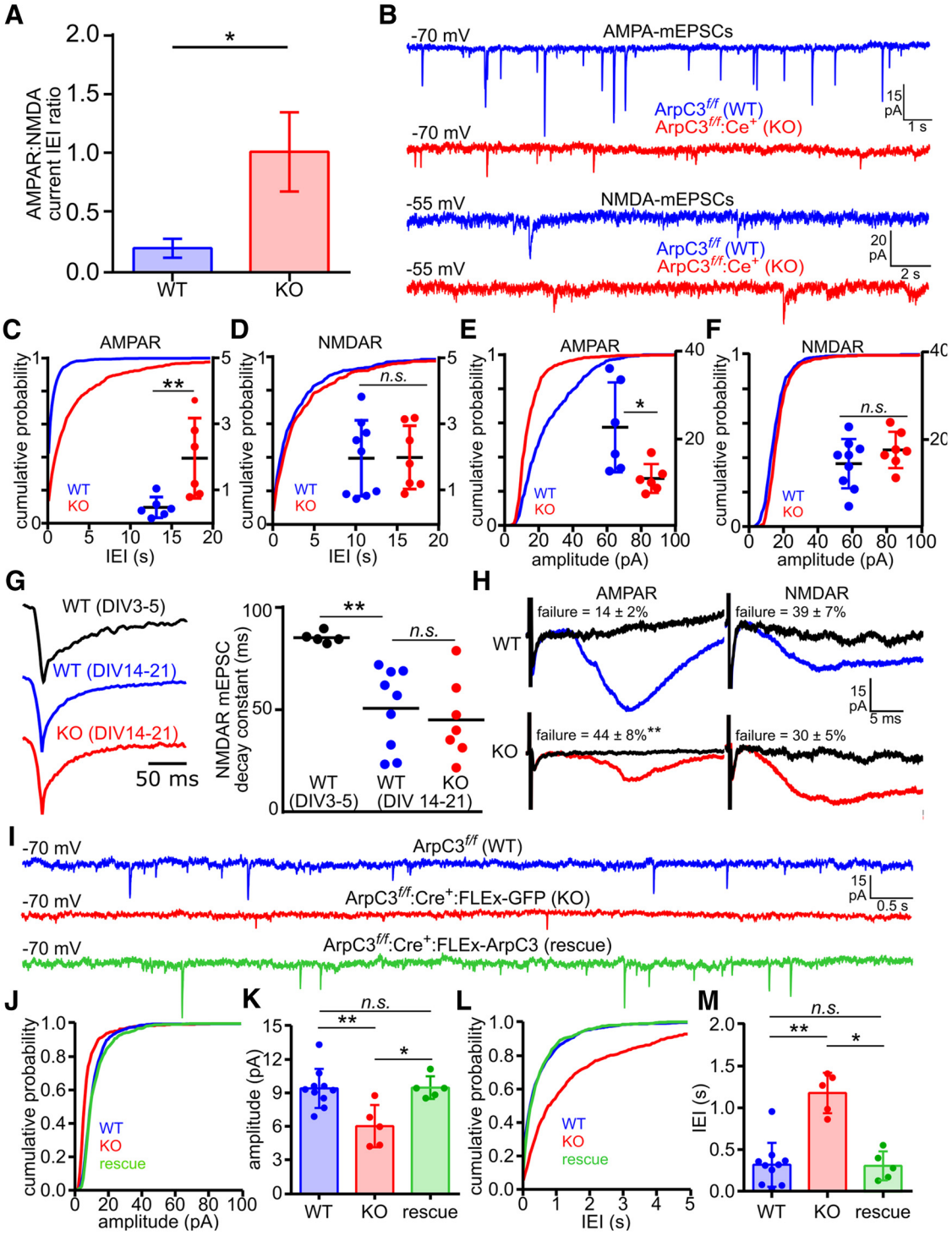

Figure 6. ArpC3-deficient synapses are functionally immature. ***A***, Effect of ArpC3 KO on AMPAR/NMDAR IEI ratios in CA1 pyramidal neurons (WT: 0.2 ± 0.2, $n = 14$; KO: 1.0 ± 0.2, $n = 12$; $p = 0.034$). ***B***, Representative traces of pharmacologically isolated AMPAR- and NMDAR-mEPSCs (as indicated) recorded from ArpC3 $^{f/f}$ (WT, blue) and ArpC3 $^{f/f}$:Cre $^{+}$ (KO, red) neurons. ***C***, ***D***, IEI cumulative probability plots for AMPAR-mEPSCs (***C***) and NMDAR-mEPSCs (***D***). Insets show median values (see right vertical axes, units are in seconds). AMPAR-mEPSC IEIs were increased in ArpC3 KO versus WT neurons (WT: 0.38 ± 0.13 s, $n = 6$; KO: 1.87 ± 0.50 s, $n = 6$; $t_{(10)} = 3.54$, $p = 0.0050$); NMDAR-mEPSC IEIs were not significantly different (WT: 1.99 ± 0.38 s, $n = 9$; KO: 2.02 ± 0.36 s, $n = 7$; $t_{(14)} = 0.043$, $p = 0.97$). ***E***, ***F***, Amplitude cumulative probability plots for AMPAR-mEPSCs (***E***) and NMDAR-mEPSCs (***F***). Insets show median values (see right vertical axes, units are in picoamperes). Compared with WT neurons, KO neurons exhibited a left-shifted AMPAR-mEPSC amplitude distribution and reduced median current amplitudes (WT: 13.1 ± 1.3 pA, $n = 6$; KO: 24.0 ± 3.9 pA, $n = 6$; $t_{(10)} = 3.00$, $p = 0.013$); the NMDAR-mEPSC amplitude distributions and median current amplitudes were comparable between groups (WT: 14.96 ± 0.89 pA, $n = 9$; KO: 16.43 ± 0.74 pA, $n = 7$; $t_{(14)} = 1.23$, $p = 0.24$). ***G***, Peak-scaled waveform averages of NMDAR-mEPSCs from WT (black, DIV3–5; blue, DIV14–21) and DIV14–21 ArpC3 KO (red) neurons. Scatter plots show that amplitude-weighted decay constants were decreased 69% from DIV 3–5 to DIV 14–21 in WT neurons (DIV 3–5: 85.5 ± 1.1 s, $n = 5$; DIV 14–21: 50.7 ± 6.5 s, $n = 9$; $t_{(12)} = 3.88$, $p = 0.0022$) but were comparable between WT and KO neurons at DIV 14–21 (KO: 45.1 ± 7.3 s, $n = 7$; $t_{(14)} = 0.58$, $p = 0.57$). ***H***, Waveform averages from minimal stimulation experiments (black, WT and KO failures; blue, WT success; red, KO success) showing selective effects of ArpC3 KO on AMPAR-mEPSC failure rates (WT: 13.5 ± 2.2%, $n = 4$; KO: 44.0 ± 7.6%, $n = 4$; $t_{(6)} = 4.46$, $p = 0.0044$) compared with NMDAR-mEPSC failures (WT: 39.2 ± 7.2%, $n = 5$; KO: 30.2 ± 5.5%, $n = 5$; $t_{(8)} = 0.99$, $p = 0.35$). ***I***, Representative traces of AMPAR-mEPSCs recorded from ArpC3 $^{f/f}$ (WT, blue), ArpC3 $^{f/f}$:Cre $^{+}$:FLEx-GFP (KO, red), and ArpC3 $^{f/f}$:Cre $^{+}$:FLEx-ArpC3 (rescue, green) neurons. ***J–M***, Cumulative probability plots and sample distributions (*Figure legend continues.*)

ArpC3 re-expression at this stage was sufficient to reverse the AMPAR-related deficits. Overall, our findings demonstrate that Arp2/3 activity is a critical factor involved in transitioning silent (i.e., AMPAR-deficient) synapses to mature, unsilenced synapses containing functional AMPARs, a process that appears to occur during the final stages of dendritic spine maturation.

Discussion

Although the actin-dependent mechanisms that regulate spine plasticity are well studied, there is comparatively less known about the regulators of actin that are important for their initial development during the postnatal period. In this study, we provide evidence that the Arp2/3 complex plays key roles in specific stages of synaptogenesis. Specifically, Arp2/3 complex is not required for initial filopodia formation but may limit the filopodial promoting activity of mDia2, which in the absence of the Arp2/3 drives an abnormal increase in dendritic filopodial density. Remarkably, in the absence of Arp2/3 activity, these filopodial-like protrusions still establish presynaptic contacts, recruit MAGUK-family scaffolding proteins, and undergo NMDAR subunit switching. However, these structures are functionally stalled at the specific transitional stage from silenced to unsilenced AMPAR-enriched spines. Finally, our data indicate that in the absence of Arp2/3, these stalled protrusions are lost over time but synaptic contacts may remain, as evidenced by comparable NMDAR IEIs. These combined results demonstrate that Arp2/3-dependent actin remodeling is essential for specific stages of spinogenesis and that the regulation of its activity is a key event in postnatal excitatory synapse formation and function.

Although dendritic spine formation is an important neurodevelopmental stage, it is still unclear how dendritic spines form. Several models have been postulated based on observations of synaptogenesis in different neuronal subtypes (Yuste and Bonhoeffer, 2004). Our data support the "filopodia" model of dendritic spine formation, in which filopodia emerge from the dendrites of neurons, make presynaptic contacts, and subsequently transition to a mature spine phenotype. In the present study, we show that if this process is stalled by loss of Arp2/3 activity, filopodial protrusions still proceed through several stages of synapse development, including the establishment of presynaptic contacts, the recruitment of MAGUKs, and the synaptic recruitment NMDA receptors. Furthermore, rescue of Arp2/3 activity recovers spine structure and function, suggesting these filopodia represent functionally immature protrusions that are otherwise competent to become spines. Additional studies in other brain regions will be required to determine whether different modes of spine formation occur in different neural subpopulations.

Although it is clear that dendritic filopodia are actin-rich structures, how actin is regulated within these structures and whether the Arp2/3 complex is involved have been open questions in the spinogenesis field (Hotulainen et al., 2009; Yang and Svitkina, 2011). Previous data have suggested two possible models for how filopodia might arise from an underlying actin cytoskeleton. In the "convergent elongation" model, filopodia emerge from a branched network of actin at the cell membrane. This model is supported by EM studies of filopodia in axonal growth cones (Korobova and Svitkina, 2008), supporting the idea that filopodia emerge from branched actin of the lamellipodia, an Arp2/3-dependent structure. Alternatively, the "tip nucleation" model suggests that actin filaments inside dendritic filopodia are created at the distal membrane by formins, independent of a pre-existing network of branched actin filaments. This model is supported by studies showing that filopodia can be induced by increased formin activity or inhibited by loss of formin activity (Schirenbeck et al., 2005; Block et al., 2008). The present findings show that dendritic filopodia form robustly in the absence of Arp2/3 activity. Hence, our results best support the tip nucleation model for filopodia formation, which would occur independently of a branched actin network. Studies in HeLa cells are also consistent with our data, wherein loss of Arp2/3 or its activator, WAVE, impairs lamellipodial formation and increases formin-dependent filopodial-like protrusions (Beli et al., 2008). Future higher-resolution microscopy examining actin structures at filopodia with and without the Arp2/3 complex are required to further understand the contextual cytoskeleton. Despite this open question, it is clear that there is some competition between the formation of Arp2/3 and formin-mediated actin structures (Beli et al., 2008). Our results showing the different expression profiles of mDia2 and WAVE suggest that dendrites may leverage this competition to shift the balance between formin-dependent filopodial formation and their subsequent Arp2/3-dependent transition into morphologically mature spines.

What are the signals that lead to the formation of a filopodium and its subsequent transformation to a stable dendritic spine? Several possible mechanisms have been proposed (Heiman and Shaham, 2010). One possibility is that the lipid bilayer recruits a cluster of factors responsible for the initiation of filopodial formation. This notion is supported by cell-free imaging of initial filopodial formation using purified factors demonstrating the initial recruitment of lipid-binding F-BAR domain proteins remodel membrane topology before the assembly of actin by Arp2/3 (Lee et al., 2010). Our previous study supports this mechanism in part, showing the F-BAR domain containing protein WRP (also termed SrGAP3) forms clusters on the dendritic shaft that facilitates initial filopodial formation by deforming the membrane (Carlson et al., 2011). Interestingly, WRP GTPase activity also reduces Rac1 activity (Soderling et al., 2007), which is consistent with our results demonstrating the genetic reduction of Rac1 enhances filopodial formation. However, in contrast to the cell-free membrane studies, our present data show that Arp2/3 activity is not required for initial dendritic filopodial formation. A second potential mechanism for filopodial formation is that dendritic filopodia and spines form in response to neurotransmitter release. This mechanism is supported by studies from mature hippocampal neurons, in which electrical stimulation of dendrites increased filopodia growth in an NMDAR-dependent manner (Maletic-Savatic et al., 1999). More recently, glutamate uncaging directly onto dendrites has also been shown to promote spine formation (Kwon and Sabatini, 2011), and the transmembrane protein syndecan-2 that is enriched in dendritic filopodia likely facilitates NMDAR-mediated, calcium-dependent maturation of filopodia to spines (Lin et al., 2007; Hu and Hsueh, 2014). We hypothesize that our data showing that

←

(*Figure legend continued.*) illustrate ArpC3's KO and rescue effects on mEPSC amplitude (ANOVA main effect: $F_{(2,20)} = 14.40$, $p < 0.001$) and IEI (ANOVA main effect: $F_{(2,20)} = 26.93$, $p < 0.001$). *Post hoc* comparisons revealed significant differences between WT and KO amplitudes (WT: 9.50 ± 0.69 pA, $n = 10$; KO: 5.97 ± 0.85 pA, $n = 5$; $p = 0.004$) and IEIs (WT: 0.26 ± 0.054 s, $n = 10$; KO: 1.19 ± 0.11 s, $n = 5$; $p = 0.003$). Whereas rescued amplitudes and IEIs were not significantly different from those of WT neurons (rescue amplitude: 9.43 ± 0.45 pA, $n = 5$; $p = 0.99$; rescue IEI: 0.32 ± 0.08 s, $n = 5$; $p = 0.92$), both values were significantly different from those of KO neurons (KO amplitude, $p = 0.02$; KO IEI, $p = 0.011$). Error bars indicate SEM; $^*p < 0.05$; $^{**}p < 0.01$.

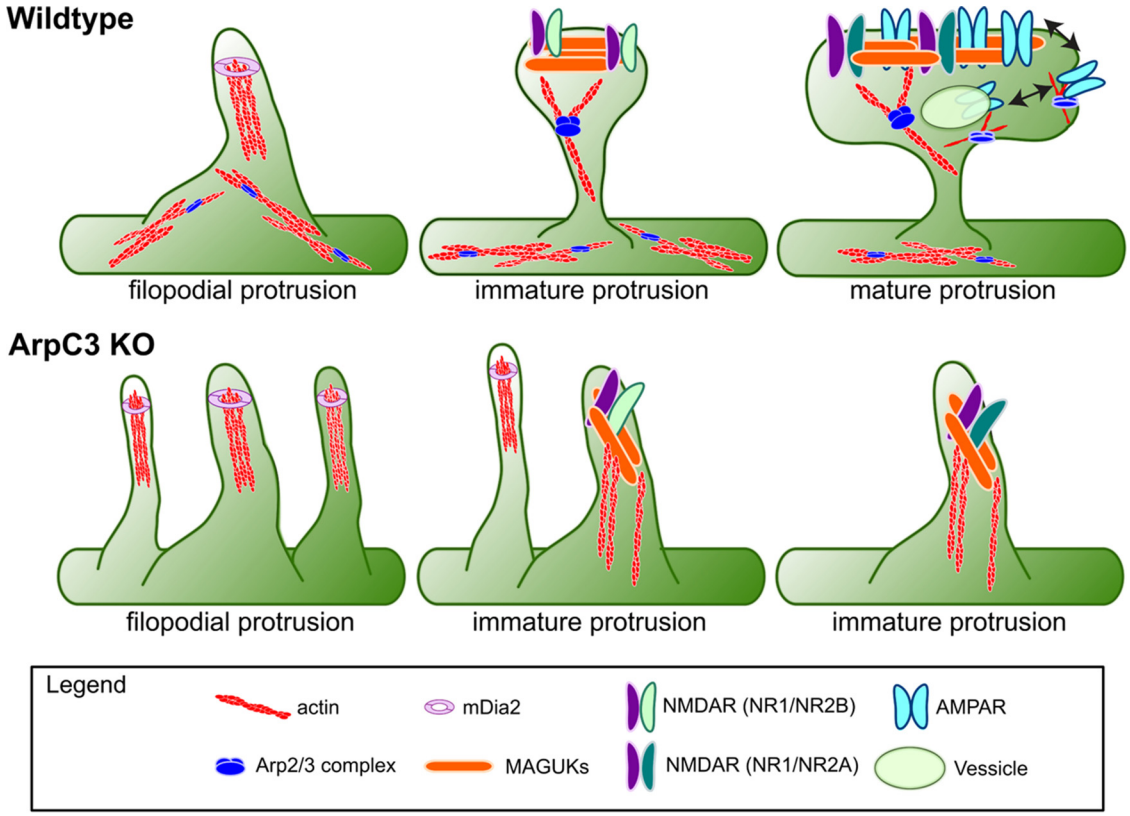

Figure 7. Schematic summarizing the roles of Arp2/3 during initial spinogenesis, morphological maturation, and AMPAR-dependent unsilencing. Initial loss of Arp2/3 activity promotes filopodia formation through mDia2-mediated linear actin nucleation. Arp2/3 is later required to mediate both the morphological enlargement of spines as well as AMPAR-dependent unsilencing of dendritic spines. Arp2/3-deficient spines, however, are able to form presynaptic contacts, undergo NMDAR subunit switching, and recruit PSD-95. Together, these data show that Arp2/3-dependent actin remodeling plays highly specialized roles in synapse formation.

Arp2/3-deficient postsynaptic contacts can recruit NMDARs best support the model in which glutamate release promotes spine maturation, although additional study is needed to substantiate this claim.

Another important mechanism for spine formation is adhesion with their presynaptic counterparts, promoting a stabilized connection between dendritic filopodia and axonal boutons. Our finding that ArpC3 $^{-/-}$ filopodia establish presynaptic contacts suggests Arp2/3 activity is not essential for synaptic adhesion. Our findings are also consistent with studies in ArpC3-null epithelia, in which loss of Arp2/3 activity had no effect on the assembly and function of the adhesive structure of the adherens junction (Zhou et al., 2013). These studies of Arp2/3 in tissue (brain and epithelia) are consistent with data supporting prominent roles for formin-dependent actin assembly in some adhesive structures (Kobielak et al., 2004; Ryu et al., 2009). We also note that although loss of ArpC3 results in fewer dendritic protrusions at DIV 17, the frequency of NMDAR currents at DIV 17–24 was not different between genotypes. This suggests that whereas dendritic protrusions collapse over time in the absence of Arp2/3 activity, synaptic adhesion is maintained via shaft synapses as we have previously reported (Kim et al., 2015). We believe that there may be two differences that occur when ArpC3 is lost during development: (1) a greater abundance of shaft synapses and (2) synapses that are AMPAR deficient. However, additional electron microscopy is needed to confirm this hypothesis. In the final stage of excitatory synaptogenesis, there is a period of postsynaptic AMPAR enrichment required for depolarization-mediated unsilencing of NMDAR activity. We note that whereas Arp2/3 is specifically required for AMPAR synaptic enrichment, it is not required for NMDA subunit switching. Although the mechanisms for AMPAR-dependent synapse unsilencing are not fully understood, the processes appear to be downstream of protein kinase A (PKA) activation (Yasuda et al., 2003), brain-derived neurotrophic factor (BDNF; Itami et al., 2003), and NMDAR-mediated calcium influx (Durand and Konnerth, 1996). Interestingly, each of these could regulate Arp2/3 activity via the Rac-WAVE pathway. For example, WAVE is known to directly scaffold PKA (Westphal et al., 2000), and the WAVE regulatory protein complex is upregulated by BDNF via TrkB (Yokota et al., 2007). Moreover, NMDAR activity resulting in Rac activity via the activation of specific Rac guanine nucleotide exchange factors (Schwechter et al., 2013) likely activates Arp2/3 in spines.

How might Arp2/3 regulate AMPAR enrichment? Our FRAP analysis suggests that there is no significant difference in initial AMPAR turnover in the absence of the Arp2/3 complex. This finding is consistent with a previous study that showed that AMPAR recovery after photobleaching was not affected by pharmacological inhibition of actin turnover (Kerr and Blanpied, 2012). Our morphology and electrophysiology rescue data also support the possibility that spine head enlargement is coupled to synaptic AMPAR recruitment (Newpher and Ehlers, 2008). We speculate that Arp2/3-dependent spine enlargement provides a critical postsynaptic density (PSD) area for AMPA receptor surface anchoring (Fig. 7). Without dendritic spine enlargement, the dramatically reduced PSD area may not be sufficient for AMPAR trapping/retention within the spine, resulting in reduced levels of synaptic AMPAR in the ArpC3 KO neurons.

In summary, this study provides the first evidence that the Arp2/3 complex plays a specific role in the developmental program of spinogenesis, including AMPAR recruitment essential for synapse unsilencing. Future work determining the factors that regulate Arp2/3 to initiate dendritic spine maturation may provide mechanistic insights into how dysfunction of the Arp2/3 signaling pathway contributes to neurodevelopmental disorders.

References

Beli P, Mascheroni D, Xu D, Innocenti M (2008) WAVE and Arp2/3 jointly inhibit filopodium formation by entering into a complex with mDia2. Nat Cell Biol 10:849–857. CrossRef Medline

Block J, Stradal TE, Hanisch J, Geffers R, Kostler SA, Urban E, Small JV, Rottner K, Faix J (2008) Filopodia formation induced by active mDia2/Drf3. J Microsc 231:506–517. CrossRef Medline

Carlson BR, Lloyd KE, Kruszewski A, Kim IH, Rodriguiz RM, Heindel C, Faytell M, Dudek SM, Wetsel WC, Soderling SH (2011) WRP/srGAP3 facilitates the initiation of spine development by an inverse F-BAR domain, and its loss impairs long-term memory. J Neurosci 31:2447–2460. CrossRef Medline

Chrostek A, Wu X, Quondamatteo F, Hu R, Sanecka A, Niemann C, Langbein L, Haase I, Brakebusch C (2006) Rac1 is crucial for hair follicle integrity but is not essential for maintenance of the epidermis. Mol Cell Biol 26:6957–6970. CrossRef Medline

Durand GM, Konnerth A (1996) Long-term potentiation as a mechanism of functional synapse induction in the developing hippocampus. J Physiol (Paris) 90:313–315. CrossRef Medline

Gallo G, Letourneau PC (2004) Regulation of growth cone actin filaments by guidance cues. J Neurobiol 58:92–102. CrossRef Medline

Gross GG, Junge JA, Mora RJ, Kwon HB, Olson CA, Takahashi TT, Liman ER, Ellis-Davies GC, McGee AW, Sabatini BL, Roberts RW, Arnold DB (2013) Recombinant probes for visualizing endogenous synaptic proteins in living neurons. Neuron 78:971–985. CrossRef Medline

Grutzendler J, Kasthuri N, Gan WB (2002) Long-term dendritic spine stability in the adult cortex. Nature 420:812–816. CrossRef Medline

Hanse E, Seth H, Riebe I (2013) AMPA-silent synapses in brain development and pathology. Nat Rev Neurosci 14:839–850. CrossRef Medline

Heiman MG, Shaham S (2010) Twigs into branches: how a filopodium becomes a dendrite. Curr Opin Neurobiol 20:86–91. CrossRef Medline

Hlushchenko I, Koskinen M, Hotulainen P (2016) Dendritic spine actin dynamics in neuronal maturation and synaptic plasticity. Cytoskeleton. Advance online publication. Retrieved August 22, 2016. doi:10.1002/cm.21280.

Hotulainen P, Llano O, Smirnov S, Tanhuanpaa K, Faix J, Rivera C, Lappalainen P (2009) Defining mechanisms of actin polymerization and depolymerization during dendritic spine morphogenesis. J Cell Biol 185:323–339. CrossRef Medline

Hu HT, Hsueh YP (2014) Calcium influx and postsynaptic proteins coordinate the dendritic filopodium-spine transition. Dev Neurobiol 74:1011–1029. CrossRef Medline

Isaac JT, Nicoll RA, Malenka RC (1995) Evidence for silent synapses: implications for the expression of LTP. Neuron 15:427–434. CrossRef Medline

Itami C, Kimura F, Kohno T, Matsuoka M, Ichikawa M, Tsumoto T, Nakamura S (2003) Brain-derived neurotrophic factor-dependent unmasking of "silent" synapses in the developing mouse barrel cortex. Proc Natl Acad Sci U S A 100:13069–13074. CrossRef Medline

Kerr JM, Blanpied TA (2012) Subsynaptic AMPA receptor distribution is acutely regulated by actin-driven reorganization of the postsynaptic density. J Neurosci 32:658–673. CrossRef Medline

Kim IH, Racz B, Wang H, Burianek L, Weinberg R, Yasuda R, Wetsel WC, Soderling SH (2013) Disruption of Arp2/3 results in asymmetric structural plasticity of dendritic spines and progressive synaptic and behavioral abnormalities. J Neurosci 33:6081–6092. CrossRef Medline

Kim IH, Rossi MA, Aryal DK, Racz B, Kim N, Uezu A, Wang F, Wetsel WC, Weinberg RJ, Yin H, Soderling SH (2015) Spine pruning drives antipsychotic-sensitive locomotion via circuit control of striatal dopamine. Nat Neurosci 18:883–891. CrossRef Medline

Kobielak A, Pasolli HA, Fuchs E (2004) Mammalian formin-1 participates in adherens junctions and polymerization of linear actin cables. Nat Cell Biol 6:21–30. CrossRef Medline

Korobova F, Svitkina T (2008) Arp2/3 complex is important for filopodia formation, growth cone motility, and neuritogenesis in neuronal cells. Mol Biol Cell 19:1561–1574. CrossRef Medline

Korobova F, Svitkina T (2010) Molecular architecture of synaptic actin cytoskeleton in hippocampal neurons reveals a mechanism of dendritic spine morphogenesis. Mol Biol Cell 21:165–176. CrossRef Medline

Kwon HB, Sabatini BL (2011) Glutamate induces de novo growth of functional spines in developing cortex. Nature 474:100–104. CrossRef Medline

Lee K, Gallop JL, Rambani K, Kirschner MW (2010) Self-assembly of filopodia-like structures on supported lipid bilayers. Science 329:1341–1345. CrossRef Medline

Liao D, Hessler NA, Malinow R (1995) Activation of postsynaptically silent synapses during pairing-induced LTP in CA1 region of hippocampal slice. Nature 375:400–404. CrossRef Medline

Lin YL, Lei YT, Hong CJ, Hsueh YP (2007) Syndecan-2 induces filopodia and dendritic spine formation via the neurofibromin-PKA-Ena/VASP pathway. J Cell Biol 177:829–841. CrossRef Medline

Lohmann C, Bonhoeffer T (2008) A role for local calcium signaling in rapid synaptic partner selection by dendritic filopodia. Neuron 59:253–260. CrossRef Medline

Maletic-Savatic M, Malinow R, Svoboda K (1999) Rapid dendritic morphogenesis in CA1 hippocampal dendrites induced by synaptic activity. Science 283:1923–1927. CrossRef Medline

Monyer H, Burnashev N, Laurie DJ, Sakmann B, Seeburg PH (1994) Developmental and regional expression in the rat brain and functional properties of four NMDA receptors. Neuron 12:529–540. CrossRef Medline

Newpher TM, Ehlers MD (2008) Glutamate receptor dynamics in dendritic microdomains. Neuron 58:472–497. CrossRef Medline

Nikonenko I, Boda B, Steen S, Knott G, Welker E, Muller D (2008) PSD-95 promotes synaptogenesis and multiinnervated spine formation through nitric oxide signaling. J Cell Biol 183:1115–1127. CrossRef Medline

Parnass Z, Tashiro A, Yuste R (2000) Analysis of spine morphological plasticity in developing hippocampal pyramidal neurons. Hippocampus 10:561–568. CrossRef Medline

Pellegrin S, Mellor H (2005) The Rho family GTPase Rif induces filopodia through mDia2. Curr Biol 15:129–133. CrossRef Medline

Peng J, Wallar BJ, Flanders A, Swiatek PJ, Alberts AS (2003) Disruption of the Diaphanous-related formin Drf1 gene encoding mDia1 reveals a role for Drf3 as an effector for Cdc42. Curr Biol 13:534–545. CrossRef Medline

Petralia RS, Sans N, Wang YX, Wenthold RJ (2005) Ontogeny of postsynaptic density proteins at glutamatergic synapses. Mol Cell Neurosci 29:436–452. CrossRef Medline

Poglia L, Muller D, Nikonenko I (2011) Ultrastructural modifications of spine and synapse morphology by SAP97. Hippocampus 21:990–998. CrossRef Medline

Ryu JR, Echarri A, Li R, Pendergast AM (2009) Regulation of cell-cell adhesion by Abi/Diaphanous complexes. Mol Cell Biol 29:1735–1748. CrossRef Medline

Schirenbeck A, Bretschneider T, Arasada R, Schleicher M, Faix J (2005) The Diaphanous-related formin dDia2 is required for the formation and maintenance of filopodia. Nat Cell Biol 7:619–625. CrossRef Medline

Schnütgen F, Doerflinger N, Calléja C, Wendling O, Chambon P, Ghyselinck NB (2003) A directional strategy for monitoring Cre-mediated recombination at the cellular level in the mouse. Nat Biotechnol 21:562–565. CrossRef Medline

Schwechter B, Rosenmund C, Tolias KF (2013) RasGRF2 Rac-GEF activity couples NMDA receptor calcium flux to enhanced synaptic transmission. Proc Natl Acad Sci U S A 110:14462–14467. CrossRef Medline

Soderling SH, Scott JD (2006) WAVE signalling: from biochemistry to biology. Biochem Soc Trans 34:73–76. CrossRef Medline

Soderling SH, Langeberg LK, Soderling JA, Davee SM, Simerly R, Raber J, Scott JD (2003) Loss of WAVE-1 causes sensorimotor retardation and reduced learning and memory in mice. Proc Natl Acad Sci U S A 100:1723–1728. CrossRef Medline

Soderling SH, Guire ES, Kaech S, White J, Zhang F, Schutz K, Langeberg LK, Banker G, Raber J, Scott JD (2007) A WAVE-1 and WRP signaling complex regulates spine density, synaptic plasticity, and memory. J Neurosci 27:355–365. CrossRef Medline

Trachtenberg JT, Chen BE, Knott GW, Feng G, Sanes JR, Welker E, Svoboda K (2002) Long-term in vivo imaging of experience-dependent synaptic plasticity in adult cortex. Nature 420:788–794. CrossRef Medline

Westphal RS, Soderling SH, Alto NM, Langeberg LK, Scott JD (2000) Scar/WAVE-1, a Wiskott-Aldrich syndrome protein, assembles an actin-associated multi-kinase scaffold. EMBO J 19:4589–4600. CrossRef Medline

Yang C, Svitkina T (2011) Filopodia initiation: focus on the Arp2/3 complex and formins. Cell Adh Migr 5:402–408. CrossRef Medline

Yang C, Czech L, Gerboth S, Kojima S, Scita G, Svitkina T (2007) Novel roles of formin mDia2 in lamellipodia and filopodia formation in motile cells. PLoS Biol 5:e317. CrossRef Medline

Yasuda H, Barth AL, Stellwagen D, Malenka RC (2003) A developmental switch in the signaling cascades for LTP induction. Nat Neurosci 6:15–16. CrossRef Medline

Yokota Y, Ring C, Cheung R, Pevny L, Anton ES (2007) Nap1-regulated neuronal cytoskeletal dynamics is essential for the final differentiation of neurons in cerebral cortex. Neuron 54:429–445. CrossRef Medline

Yuste R (2013) Electrical compartmentalization in dendritic spines. Annu Rev Neurosci 36:429–449. CrossRef Medline

Yuste R, Bonhoeffer T (2004) Genesis of dendritic spines: insights from ultrastructural and imaging studies. Nat Rev Neurosci 5:24–34. CrossRef Medline

Zhou K, Muroyama A, Underwood J, Leylek R, Ray S, Soderling SH, Lechler T (2013) Actin-related protein2/3 complex regulates tight junctions and terminal differentiation to promote epidermal barrier formation. Proc Natl Acad Sci U S A 110:E3820–E3829. CrossRef Medline

Ziv NE, Smith SJ (1996) Evidence for a role of dendritic filopodia in synaptogenesis and spine formation. Neuron 17:91–102. CrossRef Medline